

CrossMark
click for updatesCite this: *J. Mater. Chem. A*, 2015, 3,
9395Received 3rd March 2015
Accepted 11th March 2015

DOI: 10.1039/c5ta01576f

www.rsc.org/MaterialsA

The relationship between coefficient of restitution and state of charge of zinc alkaline primary LR6 batteries†

Shoham Bhadra,^a Benjamin J. Hertzberg,^b Andrew G. Hsieh,^b Mark Croft,^c
Joshua W. Gallaway,^d Barry J. Van Tassell,^e Mylad Chamoun,^f Can Erdonmez,^f
Zhong Zhong,^g Tal Shoklapper^h and Daniel A. Steingart^{*b}

The coefficient of restitution of alkaline batteries has been shown to increase as a function of depth of discharge. In this work, using non-destructive mechanical testing, the change in coefficient of restitution is compared to *in situ* energy-dispersive X-ray diffraction data to determine the cause of the macroscopic change in coefficient of restitution. The increase in coefficient of restitution correlates to the formation of a percolation pathway of ZnO within the anode of the cell, and the coefficient of restitution levels off at a value of 0.66 ± 0.02 at 50% state of charge when the anode has densified into porous ZnO solid. Of note is the sensitivity of coefficient of restitution to the amount of ZnO formation that rivals the sensitivity of *in situ* energy-dispersive X-ray diffraction.

The LR6 form factor Zn–MnO₂ battery, or the “alkaline” AA battery, accounted for \$1.8 billion of worldwide battery sales in 2013.^{1,2} The chemistry and form factor have been popular for over 50 years because of the low cost of the source material (Zn) and the bobbin cell design.³ Electrical testing is the accepted method of determining a battery’s health, but mechanical testing of batteries has surfaced as a viable method for determining the material properties of a battery. Methods have probed the mechanical behavior of the separator,^{4,5} the electrodes,^{6–10} and the entire cell.¹¹ The destructive nature of some

of these methods makes them unfeasible for applications in which the cell must remain intact. Methods such as X-ray diffraction (XRD),¹² X-ray microtomography,^{13–15} and acoustic emission sensing^{16–19} allow for non-destructive *in situ* characterization of the microstructure, but these methods require specialized equipment and, with few exceptions, cannot be applied *in operando*.

Recently there has been popular interest²⁰ in the tendency of an alkaline AA battery to bounce after being dropped on its end when discharged to full capacity, compared to a flat landing with minimal bounce when the battery is “as-received”. In this paper the coefficient of restitution (COR) of an alkaline AA battery is measured at various depths of discharge by dropping the battery in a controlled fashion and observing the subsequent bouncing, and the change in COR is then compared to spatially resolved energy-dispersive X-ray diffraction (EDXRD) that was performed *in situ* on equivalent alkaline AA batteries. Our measurements show that this simple bounce test provides a considerable amount of information of the structure of the battery’s Zn anode, rivaling the sensitivity of *in situ* EDXRD in detection of ZnO formation. This discovery shows that non-destructive acoustic testing of batteries can provide valuable information about a battery’s health and state of charge (SOC). Studies performed on other bobbin cell geometries (AAA, C and D alkaline cells) yield similar results.

To measure the COR of each LR6 alkaline AA battery, the batteries were dropped through a 25 cm tall acrylic tube onto an epoxy benchtop, coupled with a computer microphone placed 30 cm away to record the audio from each bounce, similar to the method of Stensgaard *et al.*²¹ A detailed illustration of the test setup is available in ESI Fig. 1.† The audio recording was then analyzed to determine number of bounces, height of bounce, and COR. The height of each bounce was determined by the relationship

$$h_{\text{bounce}} = \frac{1}{2}g \left(\frac{\Delta t_{\text{bounce}}}{2} \right)^2 \quad (1)$$

^aElectrical Engineering and the Andlinger Center for Energy and the Environment, Princeton University, Princeton, New Jersey 08540, USA

^bMechanical and Aerospace Engineering and the Andlinger Center for Energy and The Environment, Princeton University, Princeton, New Jersey 08540, USA

^cDepartment of Physics, Rutgers University, Piscataway, New Jersey 08854, USA

^dCity University of New York Energy Institute, New York, New York 10031, USA

^eDepartment of Chemical Engineering, City College of New York, New York, New York 10031, USA

^fSustainable Technologies Division, Brookhaven National Laboratory, Upton, New York 11973, USA

^gNational Synchrotron Light Source, Brookhaven National Laboratory, Upton, New York 11973, USA

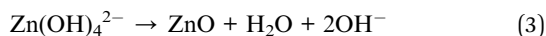
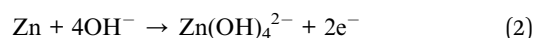
^hVoltaiq, Brooklyn, New York 11201, USA

† Electronic supplementary information (ESI) available: Materials and Methods, Audio Data, Full XRD patterns. See DOI: 10.1039/c5ta01576f

where Δt_{bounce} is the time measured between bounces with the microphone. The batteries were weighed with a lab balance (Metler-Toledo) prior to each bounce test to determine total weight, which remained constant at 23.05 ± 0.1 g. Batteries were then discharged for one hour at 280 mA, corresponding to a rate of $C/10$ (1/10 of capacity per hour) using a battery cycler (Neware BT3000-8) after each bounce test.

Electrochemical impedance spectroscopy (Gamry Reference 3000) was performed on each cell after every 280 mA h of capacity discharge. Scans were performed under potentiostatic conditions at the open circuit voltage of each cell, with an AC voltage perturbation of 10 mV, sweeping from 100 mHz to 100 kHz. EIS and bounce test data was then compared to *in situ* EDXRD data obtained at Beamline X17B1 of the National Synchrotron Light Source at Brookhaven National Laboratory. EDXRD is capable of measuring internal structural changes in a discrete volume, and a method detailed by Gallaway *et al.*¹² was employed, in which the X-ray beam was radially transmitted through each battery.

As an alkaline battery is discharged, the anode undergoes oxidation from Zn to ZnO, as seen in eqn (2) and (3), while the cathode is reduced from MnO_2 to MnOOH , shown in eqn (4).



Eqn (2) shows that the battery produces $\text{Zn}(\text{OH})_4^{2-}$ ions in solution until the electrolyte becomes supersaturated, at which point it begins to precipitate as ZnO.²²

Post mortem analysis shows that the Zn gel anode densifies into a porous, ZnO solid, as shown in Fig. 1. The densification of the anode affects the mechanical properties of the battery. The COR, which measures the elasticity of a collision between two objects, is one such mechanical property that can be determined as shown in eqn (5).

$$\text{COR} = \frac{1}{N} \sum_{n=1}^N \sqrt{\frac{h_{n+1}}{h_n}} \quad (5)$$

where N is the number of bounces, and h denotes the bounce heights determined from eqn (1). Using the bounce test described previously, the COR of alkaline batteries was measured through full discharge.

Fig. 2 shows the evolution of the COR for three identical AA cells as capacity is passed in increments of 280 mA h at 280 mA, corresponding to a rate of $C/10$. The inset shows a composited image of the corresponding drop tests for a single cell. A sharp increase in COR occurs at 80% SOC, when 560 mA h have passed, followed by asymptotic leveling of the COR at a value of 0.66 ± 0.02 after 50% SOC (1400 mA h passed). The three cells show excellent agreement in the low and high COR regimes, and the variance in the dynamic regime (80–50% SOC) shows that there is some variance from cell to cell in ZnO growth.

To show the transition between the low COR and high COR regimes more clearly, cells were discharged at 50 mA in one

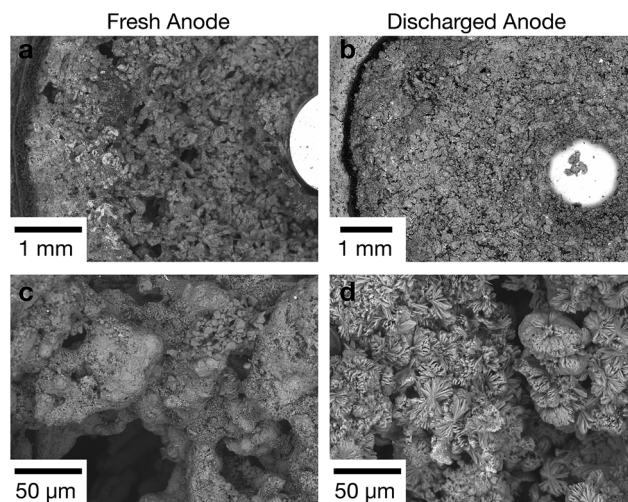


Fig. 1 (a) SEM image of “fresh” cell, where the coarse zinc gel can be seen surrounding the current collector. (b) SEM image of the same cell after full discharge (2850 mA h passed), the anode now largely converted to ZnO. A more compact morphology is seen closest to the separator, with more granular morphology near the pin. (c) High mag. SEM image showing fresh Zn particles. (d) High mag. SEM image showing coagulated ZnO particles after full discharge.

hour intervals (50 mA h) prior to bounce testing. It was found that COR is constant for low depths of discharge, rising after 450 mA h have been passed.[†] The leveling of COR for these cells occurred at 950 mA h passed, which was earlier than in cells discharged at 280 mA. It has been shown previously by Horn *et al.*²³ that lower discharge rates will result in a more even distribution of ZnO in the anode, compared to that of a higher discharge rate, thus a more even distribution of ZnO results in earlier leveling of the COR.

As the stainless steel casing does not change or partake in the electrochemical reaction, four possible effects associated with discharging an alkaline battery may be correlated with the

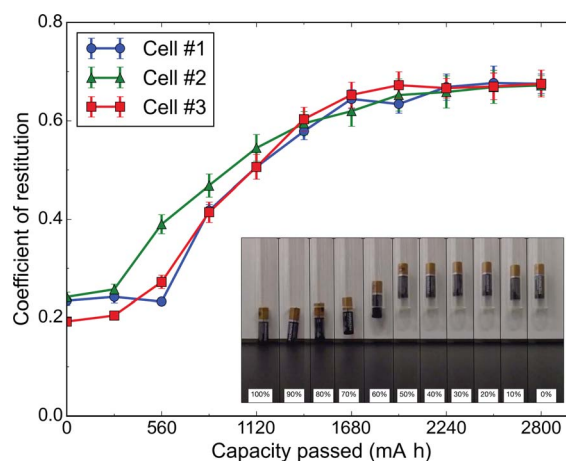


Fig. 2 Coefficient of restitution as a function of capacity passed at 280 mA. COR increases at 80% state of charge, and asymptotically levels off at 50% state of charge. Inset: composited image of bounce behavior for a single cell over full depth of discharge.

Table 1 Water content effect on coefficient of restitution

	Coefficient of restitution at 100% SOC	Coefficient of restitution at 50% SOC	Coefficient of restitution at 0% SOC
As received	0.10 ± 0.05	0.43 ± 0.02	0.43 ± 0.02
Dehydrated	0.10 ± 0.05	0.43 ± 0.02	0.42 ± 0.02
Unmodified	0.23 ± 0.02	0.60 ± 0.03	0.66 ± 0.02

observed change in COR: (1) mass loss, (2) reduction of the cathode from MnO_2 to MnOOH , (3) water consumption, and (4) oxidation of the anode from Zn to ZnO. We will discuss each of these possibilities in the remainder of the manuscript.

Mass loss can be discounted, as under all operating conditions no change was observed in the mass of each battery. The cells are effectively sealed, but have safety valves to handle H_2 generation which results from corrosion of the zinc,²² and again, no mass loss was measured during the experiments.

The EDXRD spectra for the MnO_2 cathode shows peak shifts that begin immediately upon discharge, at least 400 mA h before the onset of COR increase.† As reduction of the cathode is a linear process, it does not correlate clearly with the non-linear increase in COR. This leaves water consumption and ZnO formation. Analysis of the discharge reaction and physical properties of water, Zn, and ZnO reveals that these two aspects are strongly coupled. While the density of ZnO (5.61 g cm^{-3}) is less than that of Zn (7.14 g cm^{-3}), the density of water with 8.9 M KOH is 1.41 g cm^{-3} . Complicating the system is the use of proprietary blends of gelation agents added to the anode (typically combinations of cellulose and polyethylene glycol), so we will assume a composite density of 1.40 g cm^{-3} .²² Eqn (2)–(4) show that for every mole of Zn eventually oxidized to ZnO, and every mole of MnO_2 reduced to MnOOH , one mole of H_2O must be consumed. This means that for 2800 mA h of charge passed, 0.94 g of H_2O must be consumed during the protonation of the MnO_2 and the oxidation of the zinc.

We devised the following test to determine if water removal, without ZnO conversion, caused the increase in COR: three AA cells, one at 100% SOC (as-received), 50% SOC (half-discharged), and 0% SOC (fully-discharged), were modified by removing the top 1 cm^2 of casing, exposing both the anode and cathode. The COR of cell was then measured once before and again after dehydration in a vacuum oven at 25°C for 72 hours.

To ensure that water was removed from the entire cell (and not just the cathode), we then ran a separate test where 1 g of zinc anode gel was removed before and after desiccation. Each sample (as received and desiccated at each state of charge) was held at 80°C for 24 hours. The zinc gel, before our desiccation method, lost $0.2 \pm 0.002 \text{ g}$ when dried at 80°C in vacuum. The zinc gels, after desiccation, lost negligible (lower than the scale precision) amounts of water. This gave us confidence that water was removed through the cell during our 25°C desiccation. Additionally, the non-desiccated zinc gel could be “spread” readily with a spatula; in contrast, the desiccated zinc was rigid and would crumble when enough shear was applied to move the particles. Both were notably different from the discharged zinc, which was a rigid, concrete-like mass that was difficult to break apart.

Removing the case decreased the overall coefficient of restitution. Table 1 indicates that there was no meaningful change in the COR when the cells at different states of charge were dehydrated at 25°C for three days, despite the aforementioned water loss and “stiffening” of the anode. ESI Fig. 7† provides a visual guide to the cell before and after dehydration.

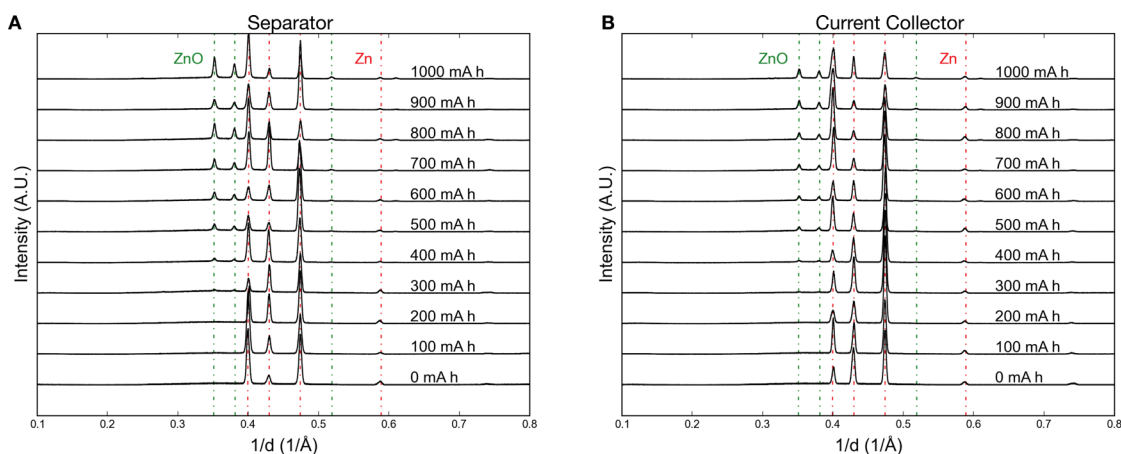


Fig. 3 EDXRD progression of anode at 100 mA discharge rate at the (a) anode–separator interface and (b) anode–current collector interfaces. ZnO peaks are denoted by green dashed lines, and Zn peaks are denoted by red dashed lines. ZnO forms at the separator before forming at the current collector.

Thus, water removal from the cell, and particularly from the zinc gel anode, alone does not alter the COR of the cell.

What is more likely the cause of the increased COR is a combination of water being consumed as zinc oxide forms as indicated by eqn (2) and (3). What we will show in subsequent sections is that while water is consumed to form zinc oxide throughout the anode, the COR change appears to correlate with the point at which ZnO is present through the thickness of the Zn gel anode.

One method for measuring the evolution of interfaces within a battery is electrochemical impedance spectroscopy (EIS).^{24,25} EIS was performed after every 10% of capacity discharged (280 mA h) to observe the effects of anode oxidation on the impedance of the battery. We found a high value for the imaginary (Z'') and real (Z') components of impedance in the as-received battery, with a two order of magnitude drop in both following 10% discharge of the cell.† This drop was most evident in the low frequency regime of the EIS spectra, often associated with mass transport limitations. We believe this high initial impedance of the cell is related to a proprietary polymeric coating on the zinc anode used in this brand of battery to improve the shelf life. It was confirmed that while other brands of AA alkaline batteries do not have this high initial electrochemical impedance, they do exhibit the same increase in COR as a function of depth of discharge. These results, while of interest, do not give a clear indication of the cause of the increase and leveling of the COR. While not crucial to our hypothesis, a detailed discussion of the EIS model that was developed is presented along with references to established EIS models in ESI Fig. 5.†

EIS suggests that some structural evolution occurs within the anode, but a method is required to characterize discrete volumes within the battery to understand the oxidation process. Recent studies have shown that performing *in situ* EDXRD on batteries during discharge can probe the evolution of the internal components.^{12–14} Using similar methods, *in situ* EDXRD was performed in AA batteries at three discharge rates: 100 mA, 200 mA, and 300 mA. The X-ray beam was incident along the width of the battery, which allows for collection of spatially resolved data, providing a measure of the oxidation of Zn to ZnO at both edges of the anode: the separator and the current collector. Fig. 3a shows that ZnO forms at the separator interface before forming at the current collector interface, shown in Fig. 3b. This trend holds for all three discharge rates.† The capacity passed at which ZnO is present at each interface is detailed in Table 2.

These spectra confirm the results of Horn *et al.*,²³ who have shown that at higher discharge rates, ZnO will grow preferentially at the separator interface before growing through the

anode towards the current collector. They have found that ZnO initially grows as a shell around the Zn particles (Type I ZnO) through dissolution-precipitation of $\text{Zn}(\text{OH})_4^{2-}$. Once the particle is completely enveloped in Type I ZnO it begins to oxidize and deposit onto the inside surface of the Type I ZnO shell *via* a second solution-precipitation step (Type II ZnO). Based on the EDXRD spectra in Fig. 3, the oxidation of Zn in the cell ultimately forms a percolation network of ZnO from the separator to the current collector, and because of the axial symmetry of the cell, detection of radial percolation also suggest percolation throughout the entire cell. This agrees well with the results of Arise *et al.*,²⁶ who have shown that following initial precipitation of ZnO onto the anode surface, the particles will coarsen and form dense films. It is also supported by the *in situ* X-ray microtomography performed by Haibel *et al.*,¹³ who show that the growth front of ZnO in an alkaline cell travels from the separator to the current collecting pin as a function of depth of discharge. Comparing the bounce test data presented in Fig. 2 with the EDXRD spectra in Fig. 3, it is clear that the formation of this percolation pathway occurs at the same time that the COR increases. This hypothesis is supported by the use of ZnO as an industrial additive to increase the COR of materials,²⁷ and previous studies performed on ceramic/metal composites (cermets),²⁸ in which increasing the ceramic content of a cermet will result in an increase in the COR, assuming the ceramic has a higher elastic modulus relative to the metal matrix. Table 3 shows relevant materials properties for the alkaline battery system. Treating the partially oxidized anode as a cermet, and knowing that the Zn to ZnO transition results in 127% increase in bulk modulus, we expect an increase in COR as the Zn particles are oxidized.

The leveling of the COR is best explained using the methods of Antonyuk *et al.*,³⁴ who have found that a material's COR will saturate at the point at which it no longer yields plastically. Using Faradaic analysis, after 1400 mA h of charge is passed (50% SOC), 1.71 g of Zn will be consumed at the anode, while 2.13 g of ZnO will be produced. At this state of charge half the Zn has been converted to ZnO, assuming a zinc limited battery, making ZnO the majority phase in the anode, both

Table 3 Materials properties

Material	Density (g cm^{-3}) ²⁹	Bulk Modulus (GPa)
Zinc (Zn)	7.05	59 (ref. 30)
Zinc oxide (ZnO)	5.06	134 (ref. 31)
Ramsdellite (MnO_2)	4.37	119 (ref. 32)
Groutite (MnOOH)	4.14	96 (ref. 33)

Table 2 Formation of ZnO within the anode

Discharge rate (mA)	Capacity passed before appearance of ZnO at separator (mA h)	Capacity passed before appearance of ZnO at current collector (mA h)
100	200–300	300–400
200	200–400	400–600
300	300–600	300–600

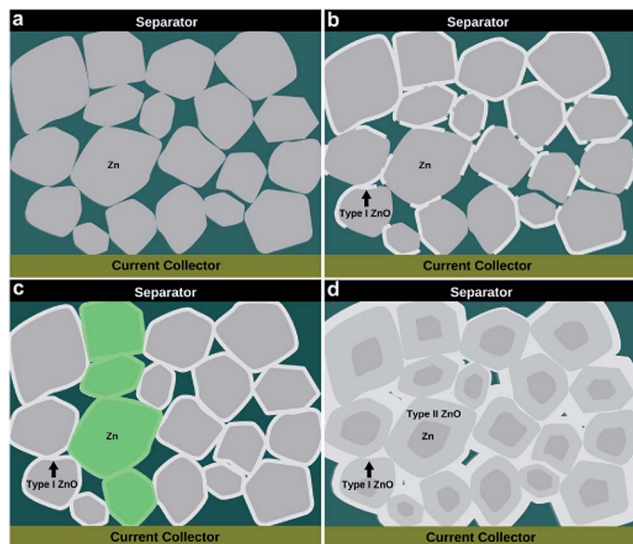


Fig. 4 The progression of ZnO formation in the anode. (a) The initial anode gel comprised of Zn particles in an electrolyte/cellulose matrix. (b) Formation of Type I ZnO shells on Zn particles. Oxidation occurs preferentially at the separator. (c) Formation of a percolation pathway. As all particles become clad in ZnO shells, a contiguous network of ZnO-clad particles forms from separator to current collector (highlighted in green). (d) Densification of the anode. Type I ZnO shells grow and Zn particles oxidize to Type II ZnO.

volumetrically and gravimetrically. As per Horn *et al.* and Arise *et al.*,^{23,26} the Type I ZnO shells will form together and sequester the liquid electrolyte while there is remaining free volume within the anode, while the bulk of the Zn particle will be oxidized to Type II ZnO. Initially, the anode gel consists of discrete Zn particles that can move within the gel matrix. Once percolation begins, this motion becomes suppressed. Once the anode densifies, as shown in Fig. 1b, it becomes a stiff ceramic core that arrests all movement of the discrete Zn particles, and the COR levels off. This process is detailed in Fig. 4, which shows the initial gel, the growth of Type I ZnO, the percolation of ZnO in the anode, and the final densification of the anode.

Conclusions

We see that determination of the COR of an alkaline battery through a simple bounce test provides an accurate measure of the morphological state of the anode. The bounce test functions as a measure of the bulk properties of a battery, as it depends on the level of oxidation of the Zn anode. After deductive analysis of the structural changes within the LR6 zinc alkaline battery, we see that the closest correlation with the beginning of the increase in COR is the consumption of water to form ZnO at the anode. As demonstrated, dehydration of the anode without ZnO network formation does not cause the battery to bounce more. However, ZnO does not form if there is no water to be consumed, so we are left to say that the bounce is most likely caused within the standard discharge mechanism by (1) the formation of ZnO by the consumption of water and (2) the point at which enough water has been consumed to form a percolated

ZnO network. It must be noted that there is still enough electrolyte to maintain low cell impedance over the entire depth of discharge: more ZnO is forming than water being lost, as a percentage of the amount of ZnO and water to begin with (roughly <0.1 g and 2.5 g, respectively).

The battery most likely begins to bounce because of displacement of water by solid ZnO bridges between particles of zinc in the gel. These bridges provide less impeding and attenuating paths for pressure waves, in turn making the battery bouncier. The sudden onset of increased COR between 400 and 600 mA h correlates strongly with EDXRD evidence of ZnO percolation, and the COR first quickly rises and then gradually tapers off near 0.66 after 1500 mA h have passed. The leveling of the COR correlates with the point at which the formation of ZnO crosses from Type I dominated to Type II dominated: whether or not this is coincidental or causal is left for a future study.

The sensitivity of the bounce test data relative to the EDXRD data is surprising, as the bounce test is capable of determining the percolation of ZnO in the anode to within 13% of the EDXRD determined value. This work shows that unconventional means of mechanical battery testing can offer knowledge of the health of a battery system at a fraction of the cost and the complexity of established methods. The results here are complementary to current electrochemical diagnostic tools, and are not meant to be a replacement of current techniques. The bounce test is a start, as future methods could incorporate a transducer/detector system in which the acoustic characteristics of a cell could be measured *in situ* without interruption of the battery system operation.

Acknowledgements

We are grateful for the patience of the Steingart lab as this work had to be carried out in a completely silent environment. We also acknowledge Sonny Moore for his contributions to drop testing in electro-acoustic applications. This work was performed with financial support from the National Science Foundation CMMI 1402872, Department of Energy ARPA-E RANGE DE-AR0000400, and the Laboratory Directed Research and Development Program of Brookhaven National Laboratory (LDRD-BNL) under Contract no. DE-AC02-98CH 10866 with the U.S. Department of Energy. Use of the National Synchrotron Light Source, Brookhaven National Laboratory, was supported by the U.S. Department of Energy, Office of Science, Office of Basic Energy Sciences, under Contract no. DE-AC02-98CH10886. The authors thank Mr. Hassan Albakri for bringing the change in bounce to our attention.

References

- 1 Highbeam Business, Primary Batteries, Dry and Wet market report, Retrieved February 26, 2014, from <http://business.highbeam.com/industry-reports/equipment/primary-batteries-dry-wet>.
- 2 Battery Manufacturing in the US, Retrieved February 28, 2014, from <http://clients1.ibisworld.com/reports/us/industry/default.aspx?entid=801>.

- 3 K. Karl, P. A. Marsal and L. F. Urry, *U. S. Pat.* no. 2,960,558, Nov 15, 1960.
- 4 J. Cannarella and C. B. Arnold, *J. Power Sources*, 2013, **226**, 149–155.
- 5 C. Peabody and C. B. Arnold, *J. Power Sources*, 2011, **196**, 8147–8153.
- 6 Y.-H. Chen, C.-W. Wang, X. Zhang and A. Sastry, *J. Power Sources*, 2010, **195**, 2851–2862.
- 7 W. Du, A. Gupta, X. Zhang, A. M. Sastry and W. Shyy, *Int. J. Heat Mass Transfer*, 2010, **53**, 3552–3561.
- 8 S. Han, J. Park, W. Lu and A. M. Sastry, *J. Power Sources*, 2013, **240**, 155–167.
- 9 J. Park, S. Kalnaus, S. Han, Y. K. Lee, G. B. Less, N. J. Dudney, C. Daniel and A. M. Sastry, *J. Power Sources*, 2013, **222**, 417–425.
- 10 K. Striebel, A. Sierra, J. Shim, C.-W. Wang and A. Sastry, *J. Power Sources*, 2004, **134**, 241–251.
- 11 J. Cannarella and C. B. Arnold, *J. Power Sources*, 2014, **245**, 745–751.
- 12 J. W. Gallaway, C. K. Erdonmez, Z. Zhong, M. Croft, L. A. Sviridov, T. Z. Sholklapper, D. E. Turney, S. Banerjee and D. A. Steingart, *J. Mater. Chem. A*, 2014, **2**, 2757–2764.
- 13 A. Haibel, I. Manke, A. Melzer and J. Banhart, *J. Electrochem. Soc.*, 2010, **157**, A387–A391.
- 14 I. Manke, J. Banhart, A. Haibel, A. Rack, S. Zabler, N. Kardjilov, A. Hilger, A. Melzer and H. Riesemeier, *Appl. Phys. Lett.*, 2007, **90**, 214102.
- 15 M. Ebner, F. Marone, M. Stampanoni and V. Wood, *Science*, 2013, **342**, 716–720.
- 16 A. Etienne, H. Idrissi, S. Meille and L. Rou, *J. Power Sources*, 2012, **205**, 500–505.
- 17 S. Kalnaus, K. Rhodes and C. Daniel, *J. Power Sources*, 2011, **196**, 8116–8124.
- 18 N. Kircheva, S. Genies, C. Chabrol and P.-X. Thivel, *Electrochim. Acta*, 2013, **88**, 488–494.
- 19 K. Rhodes, M. Kirkham, R. Meisner, C. M. Parish, N. Dudney and C. Daniel, *Rev. Sci. Instrum.*, 2011, **82**, 075107.
- 20 How to Test a AA Battery, Retrieved January 30, 2014, from http://www.youtube.com/watch?v=Y_m6p99l6ME.
- 21 I. Stensgaard and E. Laegsgaard, *Am. J. Phys.*, 2001, **69**, 301–305.
- 22 T. Reddy, *Linden's Handbook of Batteries*, McGraw-Hill Education, 4th edn, 2010.
- 23 Q. C. Horn and Y. Shao-Horn, *J. Electrochem. Soc.*, 2003, **150**, A652–A658.
- 24 D. A. Dornbusch, R. Hilton, M. J. Gordon and G. J. Suppes, *ECS Electrochem. Lett.*, 2013, **2**, A89–A92.
- 25 R. K. Ghavami, Z. Rafiei and S. M. Tabatabaei, *J. Power Sources*, 2007, **164**, 934–946.
- 26 I. Arise, S. Kawai, Y. Fukunaka and F. R. McLarnon, *J. Electrochem. Soc.*, 2013, **160**, D66–D74.
- 27 R. D. Nesbitt and M. J. Sullivan, *U. S. Pat.* no. 6,142,887, Nov 7, 2000.
- 28 I. Hussainova, J. Kbarsepp and I. Shcheglov, *Tribol. Int.*, 1999, **32**, 337–344.
- 29 W. Roberts, T. Campbell and G. Rapp, *Encyclopedia of minerals*, Van Nostrand Reinhold, 1990.
- 30 H. M. Ledbetter, *J. Phys. Chem. Ref. Data*, 1977, **6**, 1181–1203.
- 31 R. G. Munro, *NISTIR 6853*, National Institute of Standards and Technology, Gaithersburg, Maryland 20899., 2002.
- 32 Y. Lin, Y. Yang, H. Ma, Y. Cui and W. L. Mao, *J. Phys. Chem. C*, 2011, **115**, 9844–9849.
- 33 A. Suzuki, *J. Mineral. Petrol. Sci.*, 2013, **108**, 295–299.
- 34 S. Antonyuk, S. Heinrich, J. Tomas, N. G. Deen, M. S. Buijtenen and J. A. M. Kuipers, *Granular Matter*, 2010, **12**, 15–47.